

# The Galactic Mergers and Gravitational Unbound Populations

Yu-Ting Wu and Ing-Guey Jiang

*Department of Physics and Institute of Astronomy,  
National Tsing-Hua University, Hsin-Chu, Taiwan*

## ABSTRACT

Motivated by the observations on the intra-cluster light (ICL) and intergalactic stellar populations, n-body simulations are used to model the galactic merging events as a goal to investigate the production and distribution of gravitational unbound populations (GUPs). Both the parabolic and hyperbolic mergers are considered and each category includes six models with different relative orientations between two galaxies. Our results show that there are more (about a factor of two) GUP after a hyperbolic merging event than after a parabolic one. In general, depending on the relative orientation and also the relative velocity of the two galaxies in a merging pair, a head-on collision of a galaxy pair would only make a tiny fraction (less than one percent) of the initial stellar mass become luminous GUP but a considerable fraction (eight to fourteen percent) of the dark matter become dark GUP.

**Key words:** galaxies: interactions; galaxies: stellar content; galaxies: dynamics

## 1. The Introduction and Motivation

The origin of the diffused light between galaxies, as first discovered by Zwicky (1951) in the Coma cluster, has been a long term puzzle because in the standard picture, stars in the universe are formed and located within galaxies. However, Zwicky (1951)'s result implies that there are many luminous stars located between galaxies. A significant amount of stars must be far from galaxies, as implied by the brightness of the diffused light.

In order to further investigate this problem, over the years, there have been many more observations made about these inter-galactic objects. Red giants have been observed in a blank field in the Virgo Cluster as shown in Durrell et al. (2002). Planetary nebulae have been observed in the inter-galactic space of the M81 groups of galaxies (Feldmeier et al. 2004), and also in the Virgo Cluster (Ferguson et al. 1998, Arnaboldi et al. 2002) and Coma Cluster (Gerhard et al. 2005). Moreover, Gal-Yam et al. (2003) even found supernovae between galaxies.

Among these works, Durrell et al. (2002) suggested that intra-cluster stars could contribute 10% ~ 20% of the total I-band luminosity of the Virgo cluster. Furthermore, Mihos et al. (2005) recently observed Virgo cluster's core, as shown in their Figure 1 and 2, and found that there are a lot of intra-cluster stars and tidal tails between galaxies in the cluster.

With the above observational results, many interesting questions on the production of inter-galactic populations could be asked. Did these stars form through the collapse of inter-galactic medium? Are they the remnants of stellar groups during the early phase of the formation of a cluster of galaxies? Are they the outcome of continuous stripping due to the merging and interaction between galaxies? In order to obtain good answers, many theoretical studies on this subject have been done. For example, focusing on clusters of galaxies, cosmological n-body simulations have been employed to investigate the origins of intra-cluster populations (Please see Napolitano et al. 2003, Murante et al. 2004, Willman et al. 2004, Sommer-Larsen et al. 2005, Rudick et al. 2006, Murante et al. 2007). Using an observational definition of intra-cluster light (ICL) to be luminosity at a surface brightness  $\mu_V > 26.5 \text{ mag arcsec}^{-2}$ , Rudick et al. (2006) found that about 10% ~ 15% of the clusters' luminosity is at ICL surface brightness. In their simulations, the tidal stripping of cluster galaxies could be one of the main mechanisms to produce ICL. However, Murante et al. (2007) concluded that the majority of the diffused stellar component is produced during the merging in the formation history of the bright cluster galaxies.

Although inter-galactic stellar populations and the ICL have been investigated by many groups both observationally and theoretically, as reviewed in Zibetti (2008), one of the main issues is about the very definition of inter-galactic stellar populations and the ICL. All photometric studies have to define criteria, such as surface brightness thresholds etc. to isolate the light of inter-galactic stars from the galactic signal. Note that the previously mentioned work on clusters of galaxies employed different working definitions of the ICL with their own chosen criteria. However, from the dynamical point of view, the light from the stars which are not bound to any galactic potential (with dark matter included) seems to be a fundamental choice.

On the other hand, due to that van Dokkum et al. (1999) presented many examples of mergers of E/S0, or early-type spiral galaxies, Stanghellini et al.(2006) went on to study the production of inter-galactic populations through the mergers of elliptical galaxies. In their work, a pair of elliptical galaxies with a given initial mass ratio and initial relative velocity, represented by spherical distributed N-body systems, is set to have a head-on collision. The massive halo of dark matter is not considered in the above simulations. They conclude that this scenario is helpful to feed 5% ~ 20% of the total initial mass as unbound stars.

The work in Stanghellini et al.(2006) presents a good example to study the production

of gravitational unbound population (GUP) by a merging event. This types of work could compromise the cosmological n-body simulations on clusters, in the sense that (a) the detail relationship between GUP productions and the ways of merging could be investigated and (b) the members of GUP are well defined and easy to be identified in simulations. As Zibetti (2008) mentioned, in one particular system of galaxies, GUP shall be different from those photometric ICL, and to identify both of them observationally would be an important future work.

To take a further step from Stanghellini et al.(2006), we here study the merging events of spiral galaxies. The discs are used to represent the stellar components of spiral galaxies and there is no gaseous component. Thus, our model galaxies may be regarded as early-type spiral galaxies or late-type spiral galaxies in which the gaseous effect is ignored. Although ICL is our motivation for this work, we will only investigate the production of GUP here. The well-defined GUP could give strong constraint on the dynamical evolution of mergers.

Moreover, because dark matter is more massive than the stellar part (Faber 1987) and shall be dynamically important, we include the dark haloes in the systems. Indeed, the dark halo plays a crucial role in galactic dynamics. For example, Jiang & Binney (1999) demonstrated that the infall of dark matter could influence the orientation of the dark halo, and then warp the stellar disc. Jiang & Binney (2000) further showed that the dynamical friction from the Milky Way’s dark halo could successfully explain the orbit of the Sagittarius dwarf galaxy.

In the following, we describe the details of our models in §2 and present the results of our N-body simulations on mergers in §3. The conclusions are in §4.

## 2. The Model

The merging of disc galaxies is one of the most important subjects in galactic dynamics. A well-known example of merging is the interacting galaxies, NGC 4038/4039 pair, and the corresponding numerical simulations in Toomre and Toomre (1972). The improvement of computing facilities triggers many further investigations. Dubinski et al.(1996) presented an interesting study about the relation between the mass of dark haloes and the length of tidal tails in merging galaxies. Springel & White (1999) investigated the tidal tails in pairs of merging disc galaxies, from the view of cold dark matter (CDM) cosmologies. Naab, Burkert & Hernquist (1999) used the merging of disc galaxies to explain the origins of boxy and disky elliptical galaxies. Naab & Burkert (2003) performed a huge number of N-body simulations on the binary mergers of disk galaxies, in order to do a large parameter survey

and obtain the general properties. Bournaud et al. (2007) investigated the role of multiple minor mergers from the point of galaxy formation. In addition to the above, please also see more recent work in Lotz et al. (2008), Johansson et al. (2009), Thomas et al. (2009), and Naab & Ostriker (2009).

In this paper, we study the head-on mergers of spiral galaxies and their contributions on the production of GUP. A pair of galaxies with dark haloes will be employed for the simulations of merging events. Each galaxy includes two components, the stellar disc and the dark halo, with the density profiles as described in Hernquist (1993). These two components will be allowed to influence each other and relax to approach a new combined equilibrium. The parallelized version of the code, GADGET, is used for all N-body simulations (Springel et al. 2001), and the force softening is set as 0.075 kpc for both the stellar disc and dark halo.

## 2.1. The Initial Profiles

The density structure of the stellar part is

$$\rho_d(R, z) = \frac{M_d}{4\pi h^2 z_0} \exp(-R/h) \operatorname{sech}^2\left(\frac{z}{z_0}\right), \quad (1)$$

where  $M_d$  is the disc mass,  $h$  is the radial scale length, and  $z_0$  is a vertical scale length. Thus, the above function determines the initial positions of the disc particles.

On the other hand, the halo density profile is

$$\rho_h(r) = \frac{M_h}{2\pi^{3/2}} \frac{\alpha}{r_t r_c^2} \frac{\exp(-r^2/r_t^2)}{\frac{r^2}{r_c^2} + 1}, \quad (2)$$

where  $M_h$  is the halo mass,  $r_t$  is the tidal radius,  $r_c$  is the core radius, and  $\alpha$  is defined as:

$$\alpha = \{1 - \sqrt{\pi} q \exp(q^2) [1 - \operatorname{erf}(q)]\}^{-1}, \quad (3)$$

where  $q = r_c/r_t$  and  $\operatorname{erf}(q)$  is the error function as a function of  $q$ . The halo particles' initial positions are given following the above profile.

To assign initial velocities on the disc and halo particles, a rigorous procedure is used to calculate the corresponding phase-space distribution functions from the given density profiles. For spherical systems, Eddington's formula (Binney & Tremaine 1987) can be used for this purpose. Thus, as in Binney et al. (1998), we numerically calculate the halo's phase-space distribution function from  $\rho_h(r)$  and determine the halo particles' initial velocities

according to this distribution function. For non-spherical systems, such as the stellar disc, there is no analytical formula to be used to obtain the phase-space distribution function directly from the density profile. We thus have to determine the disc particles' velocities from the moments of the collision-less Boltzmann equation as in Hernquist (1993).

## 2.2. The Units

In our simulations, the unit of length is 1 kpc, the unit of mass is  $10^{10}M_{\odot}$ , the unit of time is  $9.8 \times 10^8$  years, and the gravitational constant  $G$  is 43007.1.

## 2.3. The Disc-Halo Equilibrium

There are two components in our galaxy, i.e. the stellar disc and the dark halo. Using the above units, the parameters for the galaxy are set as follows: for the dark halo,  $M_h = 32.48$ ,  $r_c = 3.5$ ,  $r_t = 35.0$ , and the number of halo particles  $N_h = 58000$ ; for the stellar disc,  $M_d = 5.6$ ,  $h = 3.5$ ,  $z_0 = 0.7$ , and the number of disc particles  $N_d = 10000$ . Because a test particle's velocity at disc's half-mass radius,  $R_{1/2} = 5.95$ , is  $v_{1/2} = 214.77$ , the dynamical time is defined to be  $T_{dyn} \equiv 2\pi R_{1/2}/v_{1/2} = 0.174$ , which is  $1.7 \times 10^8$  years.

After the construction of the N-body models of the dark halo and the stellar disc, we combine these two components to set up a disc-halo system. This system is allowed to relax to approach a new equilibrium. The total kinetic energy  $K$  and the total potential energy  $U$  are calculated, and the value of  $2K/|U|$  should be around one when the disc-halo system is in equilibrium, according to the virial theorem. We call  $2K/|U|$  the *virial ratio* from hereafter.

In Fig. 1, the virial ratio as a function of time is plotted in the top panel, and the radius enclosing 10%, 25%, 50%, 75%, 90% of the total mass, i.e. the Lagrangian radii, as a function of time are shown in the bottom panel. They show that the system approaches equilibrium at  $t = 10T_{dyn}$ . In addition, the variation of total energy is 0.013%, giving a satisfactory energy conservation. Thus, the disc-halo system at  $t = 10T_{dyn}$  of relaxation will be used to represent one of the galaxies at the beginning of a merging episode.

## 3. The N-Body Simulations

For the simulations on the merger of a pair of galaxies, the parameter space is too big to be completely explored in one paper. The initial mass ratio of the pair is fixed to be

$M_2/M_1 = 1$ , with an initial separation  $r_i = 300$  kpc and an impact parameter  $b = 0$ . Based on these parameters, the orbital energy of a merger is defined as:

$$E_{orb} \equiv \frac{1}{2} \frac{M_1 M_2}{M_1 + M_2} v_i^2 - \frac{GM_1 M_2}{r_i}, \quad (4)$$

where  $v_i$  is the initial relative velocity.

On the other hand, as shown in van Dokkum et al. (1999), there are many different possible relative angles between two discs in a merger. In order to study this effect, we choose six different relative orientations between the angular momentums of two discs. The galaxy located at  $(x, y, z) = (0, -150, 0)$  would always have an angular momentum with the direction  $\hat{L}=(0, 0, 1)$ , but the galaxy at  $(x, y, z) = (0, 150, 0)$  would have an angular momentum with six different directions. For parabolic (hyperbolic) mergers, the galaxy at  $(x, y, z) = (0, 150, 0)$  would have an angular momentum with direction  $\hat{L}_1=(0, 0, 1)$  in Model P1 (H1),  $\hat{L}_2=(0, -1, 0)$  in Model P2 (H2),  $\hat{L}_3=(0, 0, -1)$  in Model P3 (H3),  $\hat{L}_4=(0, 1, 0)$  in Model P4 (H4),  $\hat{L}_5=(1, 0, 0)$  in Model P5 (H5),  $\hat{L}_6=(-1, 0, 0)$  in Model P6 (H6), respectively. The discs of two galaxies are said to be parallel in Model P1 (H1), anti-parallel in Model P3 (H3), and perpendicular in the rest models.

### 3.1. The Parabolic Mergers

For the parabolic mergers, the initial orbital energy  $E_{orb} = 0$ . Thus, the two galaxies of the parabolic mergers have an initial relative velocity  $v_i = 147.8$  km/s.

#### 3.1.1. Evolution

Fig. 2(a) shows the virial ratio,  $2K/|U|$ , of the galaxy pair (with dark haloes) as a function of time for Model P1 during  $t=0 \sim 39T_{dyn}$  ( $T_{dyn}$  is the dynamical time). There are strong interactions between two galaxies during  $t=5 \sim 15T_{dyn}$ , so that the virial ratio goes away from one. The first peak of  $2K/|U|$  is around  $t = 8T_{dyn}$  and the 2nd peak is around  $t = 10T_{dyn}$ . The minimum of  $2K/|U|$  is around  $t = 9T_{dyn}$ .

On the other hand, Fig. 2(b) shows the distance between two stellar components of the galaxies during the merging. We plot the center of mass of each stellar component as a function of time in Model P1. The location of each stellar component in this plot is defined by the center of mass of its particles. Indeed, the first close encounter happens at  $t = 8T_{dyn}$  and the 2nd one is at  $t = 10T_{dyn}$ . In between these two encounters, the stellar components

of two galaxies are well separated at  $t = 9T_{dyn}$ . After  $t = 10T_{dyn}$ , two galaxies are merged and a merger has formed.

The initial relative orientation of discs in a merger does not affect the timing of principle dynamical processes, so that the corresponding plots of other parabolic models are similar with Fig. 2 and not shown here. However, the particle distributions of the stellar components in the mergers are different in these models as shown in Fig. 3. Using Model P1 as an example, Fig. 4 shows the distribution of stellar particles on the  $x - y$  plane at different times. Initially, at  $t = 0$ , two discs are well separated by 300 kpc. They come a bit closer at  $t = 4T_{dyn}$  and merge at  $t = 8T_{dyn}$ . After a violent mixing process from  $t = 9$  to  $10T_{dyn}$ , the two systems combine to approach a new equilibrium after  $t=15$ , and some particles escape far from the central part, as shown at  $t = 27$  and  $39T_{dyn}$ .

The dark-matter-particle distributions in the mergers of Model P1-P6 are shown in Fig. 5. Fig. 6 shows the distribution of dark halo particles in Model P1. At  $t = 4T_{dyn}$ , the two haloes are very close and almost touching. They are merged between  $t = 8$  and  $9T_{dyn}$ , expanding further from  $t = 10$  to  $15T_{dyn}$ . The outer part expands even further, causing some particles to escape from the system.

In Fig.3-6, the blue dots represent the unbound particles which were belong to the galaxy initially located at  $(x, y, z) = (0, -150, 0)$ , and the pink dots represent the unbound particles which were belong to another galaxy.

### 3.1.2. The Density Profiles

In order to understand the distribution of the stellar particles of the merger, we calculate the mass density of stellar particles as a function of  $r$ , where  $r$  is the distance from the center of mass of all stellar particles. Fig. 7(a) gives the density profiles of the stellar components in the models of the parabolic mergers at  $t = 39T_{dyn}$ . It shows that the central density yielded from Model P1 is higher than that which is yielded by Model P2-P6. The central density given by Model P3 is very low, indicating that the whole system is stretched out. The central densities given by other models are in between.

Fig. 7(b) shows the percentage of accumulated stellar mass as a function of  $r$ . For the region with  $r < 3$ , the solid curve (Model P1) is at the top and the short-dashed curve (Model P3) is at the bottom, which is consistent with the results shown in Fig. 7(a). However, near  $r = 20$ , all the curves approach similar values.

On the other hand, Fig. 7(c) and 7(d) give the density profiles and the percentage of

accumulated mass for the dark matter. They show that the differences between models are smaller than the corresponding ones for the stellar components in Fig. 7(a)-(b).

### 3.1.3. The Gravitational Unbound Population

We calculate the total energy of both stellar and dark-matter particles, in order to identify the GUP, and then determine their fractions. In Table 1, the first row gives the percentage of stellar GUP particles (compared to the total number of stellar particles) and the 2nd row lists the percentage of dark-matter GUP particles (compared to the total number of dark-matter particles) at  $t = 39T_{dyn}$  in parabolic mergers. For the stellar GUP, the average percentage is  $m_{P_s} = 0.1583$ , and the standard deviation is  $\sigma_{P_s} = 0.0524$ . Almost all values are within or near the boundary of the interval  $[m_{P_s} - \sigma_{P_s}, m_{P_s} + \sigma_{P_s}] = [0.1059, 0.2107]$ . For the dark-matter GUP, the mean is  $m_{P_d} = 7.7883$  with a standard deviation  $\sigma_{P_d} = 0.0508$ . The interval  $[m_{P_d} - \sigma_{P_d}, m_{P_d} + \sigma_{P_d}] = [7.7375, 7.8391]$  Only the dark-matter GUP of Model P6 is a bit smaller and has a value about  $m_{P_d} - 2\sigma_{P_d}$ .

Model	P1	P2	P3	P4	P5	P6
stellar GUP (%)	0.16	0.10	0.18	0.08	0.22	0.21
dark-matter GUP (%)	7.84	7.80	7.83	7.76	7.81	7.69

Table 1: The percentages of stellar GUP and dark-matter GUP in parabolic mergers.

## 3.2. The Hyperbolic Mergers

In order to examine the effects of larger relative velocities in a merging event, we here investigate hyperbolic mergers, in which the orbital energy  $E_{orb} > 0$ . We model six hyperbolic mergers with different relative orientations. All the parameters of the hyperbolic mergers are the same as in the parabolic mergers, except that we assume the initial relative velocities of merging galaxies in these models (Model H1-H6) to be  $v_{max}$ , which can be calculated from (Binney & Tremaine 1987)

$$v_{max} = 1.2\sqrt{\langle v^2 \rangle}, \quad (5)$$

where  $\langle v^2 \rangle$  is the mean-square velocity of all particles in one galaxy (both stellar and dark components are included). If the relative velocity between two galaxies is larger than  $v_{max}$ , it is likely that they will penetrate through each other, and cannot combine to be a merger. Using  $v_{max}$  as the initial relative velocity would highlight the effects of the larger relative merging velocity. We find that  $v_{max}$  is equal to 273.1 km/s for our system.



Using the model with anti-parallel discs as an example, Fig. 8(a) shows the virial ratio,  $2K/|U|$ , of one merging system (including both stellar and dark components) as a function of time for Model H3 during  $t=0 \sim 39T_{dyn}$ . There are direct collisions and strong interactions between two galaxies, so that the virial ratio  $2K/|U|$  goes far from 1. It shows that the first peak of  $2K/|U|$  is about  $t = 5T_{dyn}$  and the 2nd peak is about  $t = 10T_{dyn}$ . The minimum of  $2K/|U|$  is about  $t = 8T_{dyn}$ .

Moreover, Fig. 8(b) shows the distance between two stellar components of the galaxies during the merging of Model H3. The first close encounter happens at  $t = 5T_{dyn}$ , and then two galaxies move away from each other until  $t = 8T_{dyn}$ , at which they are separated for more than 60 kpc. They collide again at  $t = 10T_{dyn}$  and get mixed together afterward. The corresponding plots of other hyperbolic mergers are similar with the above, thus are not shown in the paper. The distributions of stellar particles on the  $x - y$  plane for Model H1-H6 are shown in Fig. 9. Using Model H3 (Fig. 10) as an example, at  $t = 0$ , two discs are well separated by 300 kpc. They get closer at  $t = 2T_{dyn}$  and soon merge at  $t = 5T_{dyn}$ . The violent mixing processes from  $t = 8$  to  $10T_{dyn}$  produce a complicated structure, due to that the spins of two discs are completely opposite initially. The system approaches equilibrium gradually and some particles escape far from the central part of the merger, as shown at  $t = 15, 27, \text{ and } 39T_{dyn}$ . The dark-matter-particle distributions in the mergers of Model H1-H6 at  $t = 39T_{dyn}$  are shown in Fig. 11 and the distributions of dark halo particles of Model H3 at different times are shown in Fig. 12. The halo expands slightly larger than the ones in the parabolic mergers.

Here we also calculate the mass density of stellar particles in each spherical shell and obtain the density of the stellar component as a function of  $r$ . Fig. 13(a) shows the density profiles of stellar components in Model H1-H6 at  $t = 39T_{dyn}$ . It shows that the central density of Model H1 is higher than that of other models. The central density of Model H3 and H6 are lower, indicating that the systems are stretched out. The central densities of other models are in between.

Fig. 13(b) gives the percentage of accumulated stellar mass as a function of  $r$  for each considered model. For the region with  $r < 3$ , the solid curve (Model H1) is at the top and the short-dashed curve (Model H3) is at the bottom. However, near  $r = 25$ , all the curves approach to a similar value. Fig. 13(c)-(d) are the corresponding plots for the dark matter, and the deviations between curves are smaller than those in Fig. 13(a)-(b).

In Table 2, we list the percentages of stellar GUP (the first row) and dark-matter GUP (the second row) at  $t = 39T_{dyn}$  in hyperbolic mergers. For the stellar GUP, the average percentage is  $m_{Hs} = 0.3183$ , and the standard deviation is  $\sigma_{Hs} = 0.0809$ . The first interval  $[m_{Hs} - \sigma_{Hs}, m_{Hs} + \sigma_{Hs}] = [0.2374, 0.3992]$ , and the second interval  $[m_{Hs} - 2\sigma_{Hs}, m_{Hs} + 2\sigma_{Hs}] =$

[0.1565, 0.4801]. The stellar GUPs of Model H1, H5, H6 are within the first interval, and the ones of Model H2, H3, H4 are within the second interval. For the dark-matter GUP, the mean is  $m_{Hd} = 14.1517$  with a standard deviation  $\sigma_{Hd} = 0.1446$ . The  $1\sigma$  interval  $[m_{Hd} - \sigma_{Hd}, m_{Hd} + \sigma_{Hd}] = [14.0071, 14.2963]$  and  $2\sigma$  interval  $[m_{Hd} - 2\sigma_{Hd}, m_{Hd} + 2\sigma_{Hd}] = [13.8625, 14.4409]$ . Thus, the values of Model H1, H2, H5, H6 are in  $1\sigma$  interval, and the ones of Model H3, H4 are within  $2\sigma$  interval approximately.

Model	H1	H2	H3	H4	H5	H6
stellar GUP (%)	0.37	0.21	0.42	0.21	0.33	0.37
dark-matter GUP (%)	14.22	14.12	14.33	13.86	14.19	14.19

Table 2: The percentages of stellar GUP and dark-matter GUP in hyperbolic mergers.

### 3.3. The Credibility Tests

N-body simulations have been used as powerful tools to study the dynamical evolution of galaxies, and thus have helped to gain many important implications in this field. However, technically, the detail setting of models would in general lead to different numerical results. In N-body simulations of galaxies, one would usually concern that how the results vary with the force softening parameter and total number of particles.

In order to address this point, we have done three additional testing simulations, which would be called Run A, B, C. These three have different softening parameters or total number of particles. For the simulations in Model P1-P6 and H1-H6, the total number of particles used in one merging event (consisting two galaxies) is 136000, the force softening parameters of both stellar disc and dark halo are set to be 0.075 kpc. We now define  $N_M = 136000$ ,  $S_M = 0.075$  kpc. All the details of testing simulations are the same as in Model P1 except the values of total number of particles and softening parameters.

Table 3 shows the details of testing simulations, i.e. Run A, B, C, where  $N_T$  means the total number of particles used in one merging event,  $S_h$  means the softening parameter of dark halo, and  $S_d$  means the softening parameter of disc component.

The main results of Run A, B, C are also listed in Table 3, where  $\delta E/E$  means the percentage of energy variation over whole merging event, up to  $t = 39T_{dyn}$ . To be convenient, the corresponding details and results of Model P1 are also listed at the bottom of Table 3.

At first, in Run A, the total number of particles is the same as in Model P1, but the

	$N_T$	$S_h$	$S_d$	$\delta E/E$ (%)	Stellar GUP (%)	Dark GUP (%)
Run A	$1N_M$	$5S_M$	$5S_M$	1.415	0.195	7.81
Run B	$1N_M$	$5S_M$	$1S_M$	1.375	0.205	7.87
Run C	$5N_M$	$1S_M$	$1S_M$	1.160	0.180	7.98
Model P1	$1N_M$	$1S_M$	$1S_M$	0.800	0.160	7.84

Table 3: The testing simulations: Run A, B, C.

softening parameters,  $S_h$  and  $S_d$  are five times larger than the values used in Model P1. This is to test the effect of larger softening parameters while we keep that the halo and disc have the same value, i.e.  $S_h = S_d$ . We find that  $\delta E/E$  is slightly larger, the stellar GUP increases 0.035 percent, and the dark GUP decreases 0.03 percent.

Secondly, in Run B, the total number of particle and the disc softening parameter are the same as in Model P1, but the halo softening parameter is now set to be five times larger than the disc softening parameter. This is to test the effect that the halo and disc components have different softening parameters. We find that  $\delta E/E$  increases a bit, the stellar GUP increases 0.045 percent, and the dark GUP also increases 0.03 percent, comparing with the results of Model P1.

Finally, in Run C, both the halo and disc softening parameters are the same as in Model P1, but the total number of particles is now five time of the one in Model P1. This is to test the effect of total number of particles. We find that  $\delta E/E = 1.160$ , the stellar GUP increases 0.02 percent, and the dark GUP also increases 0.14 percent, comparing with the results of Model P1.

To summarize, these testing simulations show that the numerical variation of stellar GUP ranges from 0.02 to 0.045 percent, and the one of dark GUP ranges from -0.03 to 0.14 percent due to the effects of softening parameters and total number of particles. Comparing with the values in Model P1, the fractions of variations range from 0.02/0.160 to 0.045/0.160, i.e. 0.125 to 0.281 for the stellar GUP, and from -0.03/7.84 to 0.14/7.84, i.e. -0.00383 to 0.01786 for the dark GUP. The larger uncertainty for stellar GUP is due to the small number of stellar GUP particles.

#### 4. Concluding Remarks

In order to investigate the relationship between the galactic mergers and GUP, we have used the combined disc-halo systems to model the head-on merging events of spiral galaxies.

We consider both the parabolic and hyperbolic mergers, and we propose six models for each of the mergers, with different relative orientations between two merging galaxies.

Our results show that the timing of the merging process does not depend on the relative orientation. Nevertheless, the resulting structures of stellar components show a great variety for different disc orientations.

In terms of the production of GUP, we found that head-on merging events produce much more dark-matter GUP than the stellar GUP. This could be due to that the stellar particles are initially located at the very central part of whole systems, and thus more difficult to become gravitational unbound. On the other hand, the dark-matter particles distribute over a large range, and those initially located at the outer part could be striped out of the system easily.

Moreover, due to the higher energy injection rate of the hyperbolic merging process, it produces more GUP than the parabolic one (about a factor of two). To understand the production of GUP at different times, in Fig. 14(a)-(d), we plot the percentage of stellar GUP as a function of time. It shows that, in Model P1-P6, the merging event starts to produce GUP quickly at  $t = 8T_{dyn}$ , which is actually the time when the first encounter happens. After  $t = 10T_{dyn}$ , very little stellar GUP particles are produced. In Model H1-H6, the production starts at  $t = 5T_{dyn}$ . The production rate is very high from  $t = 5T_{dyn}$  to  $t = 6T_{dyn}$ . Then, the stellar GUP slowly increases until  $t = 15T_{dyn}$ . Similarly, the corresponding plots for the dark-matter GUP are shown in Fig. 14(c)-(d). Therefore, the energy injection rate is essential for the production of GUPs. In order to visualize these GUPs, the final distributions of stellar GUP were shown in Fig. 3 and Fig. 9 and dark-matter GUP particles are shown in Fig. 5 and Fig. 11, respectively.

On the other hand, we also calculated the mean and standard deviation of GUP percentages. For parabolic mergers, the GUP percentages are all within or close to the boundary of  $1\sigma$  interval. For hyperbolic mergers, some model's GUP percentages are in  $1\sigma$  interval but some others are inside or near the boundary of  $2\sigma$  interval. Therefore, in addition to producing more GUP, the hyperbolic mergers also show larger scattering in terms of GUP production.

In general, our results show that, depending on the relative orientation and the relative velocity, a head-on collision of a galaxy pair (with dark matter) would make less than one percent of the initial stellar mass become the luminous GUP but about eight to fourteen percent of the dark matter become the dark GUP. Therefore, multiple mergers are needed to produce much more stellar GUPs.

### **Acknowledgment**

We owe a debt of thanks to the anonymous referee for good suggestions that improved the paper enormously. We also thank the National Center for High-performance Computing for computer time and facilities. This work is supported in part by the National Science Council, Taiwan, under NSC 97-2112-M-007-005.

## REFERENCES

- Arnaboldi, M., Aguerri, J. A. L., Napolitano, N. R., Gerhard, O., Freeman, K. C., Feldmeier, J., Capaccioli, M., Kudritzki, R. P., Mendez, R. H., 2002, *AJ*, 123, 760
- Binney, J., Jiang, I.-G., Dutta, S.N., 1998, *MNRAS*, 297, 1237
- Binney, J., & Tremaine, S., 1987, *Galactic Dynamics* (Princeton University Press)
- Bournaud, F., Jog, C. J., Combes, F., 2007, *A&A*, 476, 1179
- Dubinski, J., Mihos, J. C., Hernquist, L., 1996, *ApJ*, 462, 576
- Durrell, P. R., Ciardullo, R., Feldmeier, J. J., Jacoby G. H., & Sigurdsson, S., 2002, *ApJ*, 570, 119
- Faber, S. M., 1987, *Nearly Normal Galaxies: From the Planck Time to the Present; Proceedings of the Eighth Santa Cruz Summer Workshop in Astronomy and Astrophysics*, Springer-Verlag, New York
- Feldmeier, J. J., Ciardullo, R., Jacoby, G. H., Durrell, P. R., 2004, *ApJ*, 615, 196
- Ferguson, H. C., Tanvir, N. R., von Hippel, T., 1998, *Nature*, 391, 461
- Gal-Yam, A., Maoz, D., Guhathakurta, P., Filippenko, A. V., 2003, *AJ*, 125, 1087
- Gerhard, O., Arnaboldi, M., Freeman, K. C., Kashikawa, N., Okamura, S., Yasuda, N., 2005, *ApJ*, 621, L93
- Hernquist, L., 1993, *ApJS*, 86, 389
- Jiang, I.-G., Binney, J., 1999, *MNRAS*, 303, L7
- Jiang, I.-G., Binney, J., 2000, *MNRAS*, 314, 468
- Johansson, P. H., Naab, T., Burkert, A., 2009, *ApJ*, 690, 802
- Lotz, J. M., Jonsson, P., Cox, T. J., Primack, J. R., 2008, *MNRAS*, 391, 1137
- Mayer, L., Governato, F., Colpi, M., Moore, B., Quinn, T., Wadsley, J., Stadel, J., & Lake, G., 2001, *ApJ*, 547, L123
- Merritt, D., 1984, *ApJ*, 276, 26
- Mihos, J. C., Harding, P., Feldmeier, J., & Morrison, H., 2005, *ApJ*, 631, L41

- Moore, B., Katz, N., Lake, Ge., Dressler, A., & Oemler, A., 1996, *Nature*, 379, 613
- Murante, G. et al., 2004, *ApJ*, 607, L83
- Murante, G. et al., 2007, *MNRAS*, 377, 2
- Naab, T., Burkert, A., 2003, *ApJ*, 597, 893
- Naab, T., Burkert, A., Hernquist, L., 1999, *ApJ*, 523, L133
- Naab, T., Ostriker, J. P., 2009, *ApJ*, 690, 1452
- Napolitano, N. R. et al., 2003, *ApJ*, 594, 172
- Rudick, C. S., Mihos, J. C., McBride, C., 2006, *ApJ*, 648, 936
- Sommer-Larsen, J., Romeo, A. D., Portinari, L., 2005, *MNRAS*, 357, 478
- Springel, V., White, S. D. M., 1999, *MNRAS*, 307, 162
- Springel, V., Yoshida, N., & White, S.D.M., 2001, *NewA*, 6, 79
- Stanghellini, L., Gonzalez-Garcia, A. C., & Manchado, A., 2006, *ApJ*, 644, 843
- Thomas, J., Jesseit, R., Saglia, R. P., Bender, R., Burkert, A., Corsini, E. M., Gebhardt, K., Magorrian, J., Naab, T., Thomas, D., Wegner, G., 2009, *MNRAS*, 393, 641
- Toomre, A., Toomre, J., 1972, *ApJ*, 460, 121
- van Dokkum, P. G., Franx, M., Fabricant, D., Kelson, D. D., Illingworth, G. D., 1999, *ApJ*, 520, L95
- Willman, B., Governato, F., Wadsley, J., Quinn, T., 2004, *MNRAS*, 355, 159
- Zibetti, S., 2008, *Proceedings of the IAU Symposium*, 244, 176
- Zwicky, F., 1951, *PASP*, 63, 61

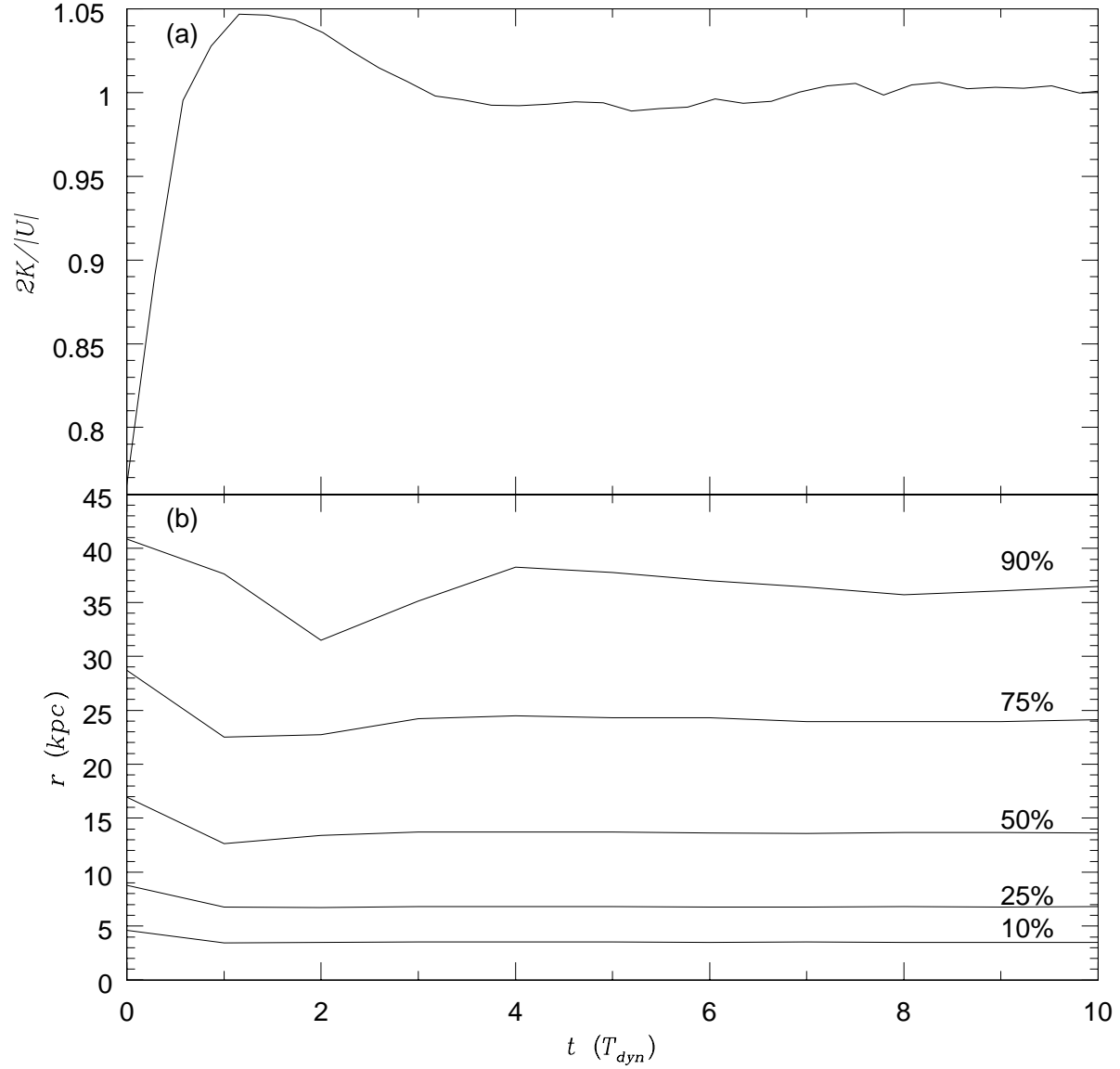


Fig. 1.— The virial ratio  $2K/|U|$  (top panel) and Lagrangian radii (bottom panel) of the disc-halo system as a function of time  $t$ , where the unit of  $t$  is the dynamical time  $T_{dyn}$ .



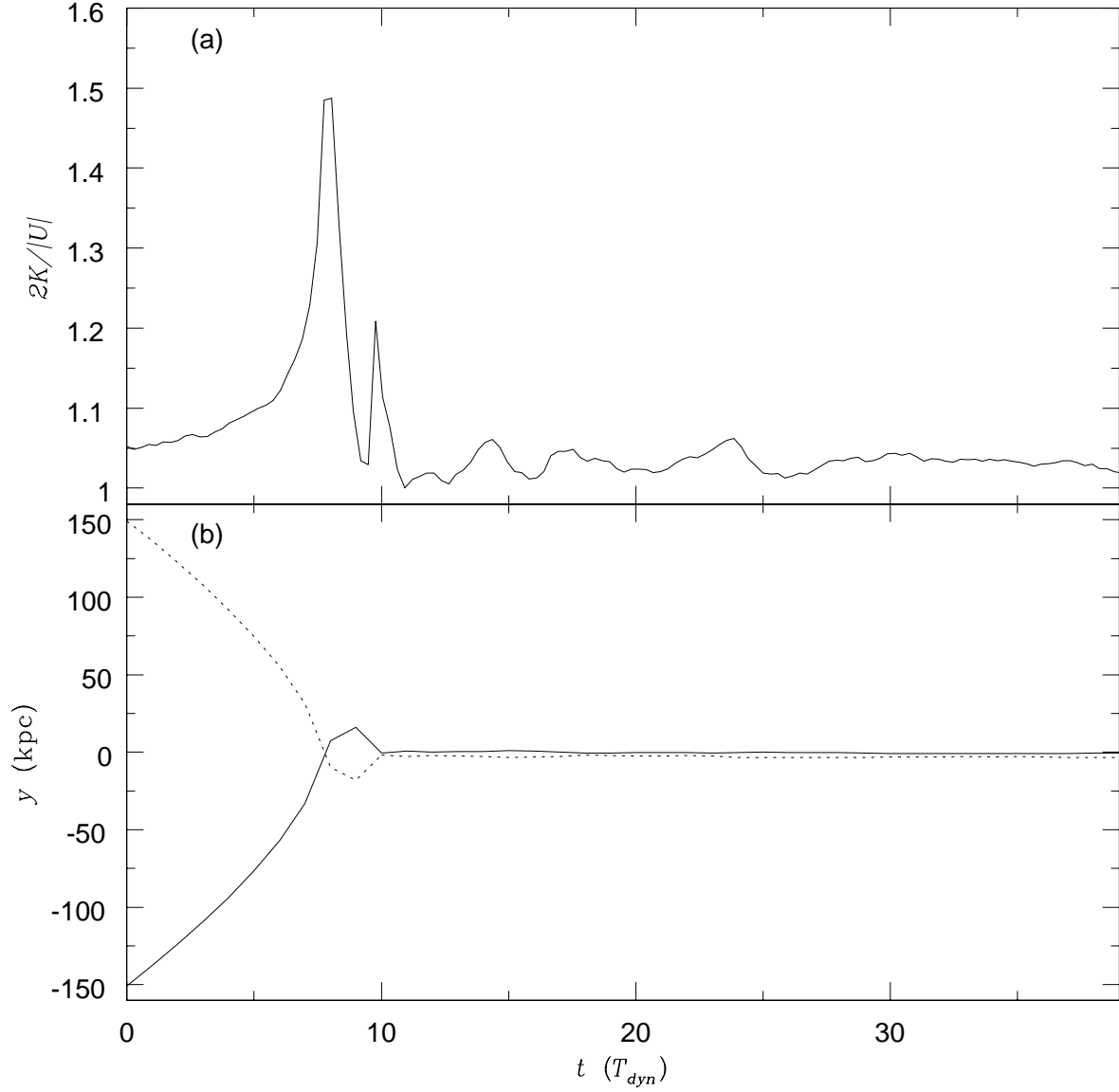


Fig. 2.— The evolution of Model P1. (a) The virial ratio  $2K/|U|$  of the merger as a function of time  $t$ . (b) The distance between two stellar components as a function of time during the merging process, where the solid and dotted curves are for the locations of two stellar components.

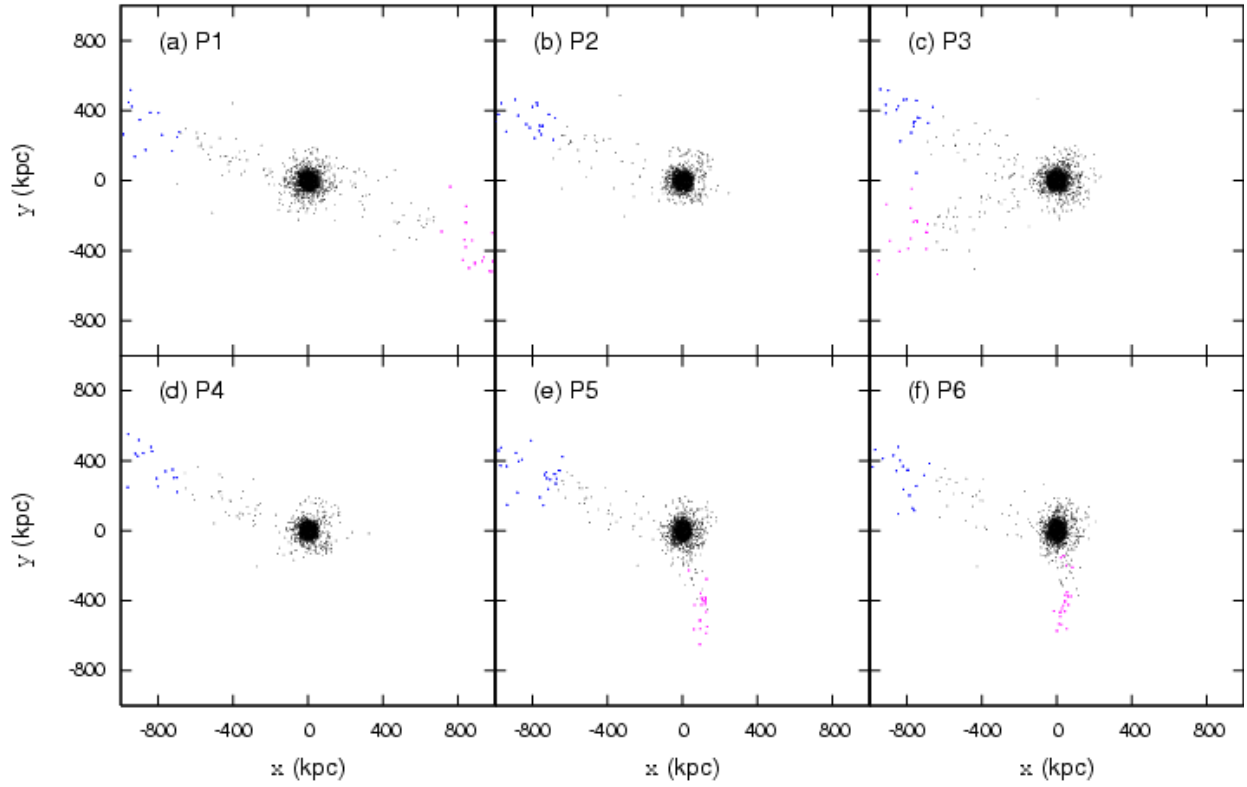


Fig. 3.— The distributions of stellar particles on the  $x - y$  plane at  $t = 39T_{dyn}$  in Model P1-P6. The blue dots represent the unbound particles which were belong to the galaxy initially located at  $(x, y, z) = (0, -150, 0)$ , and the pink dots represent the unbound particles which were belong to another galaxy.

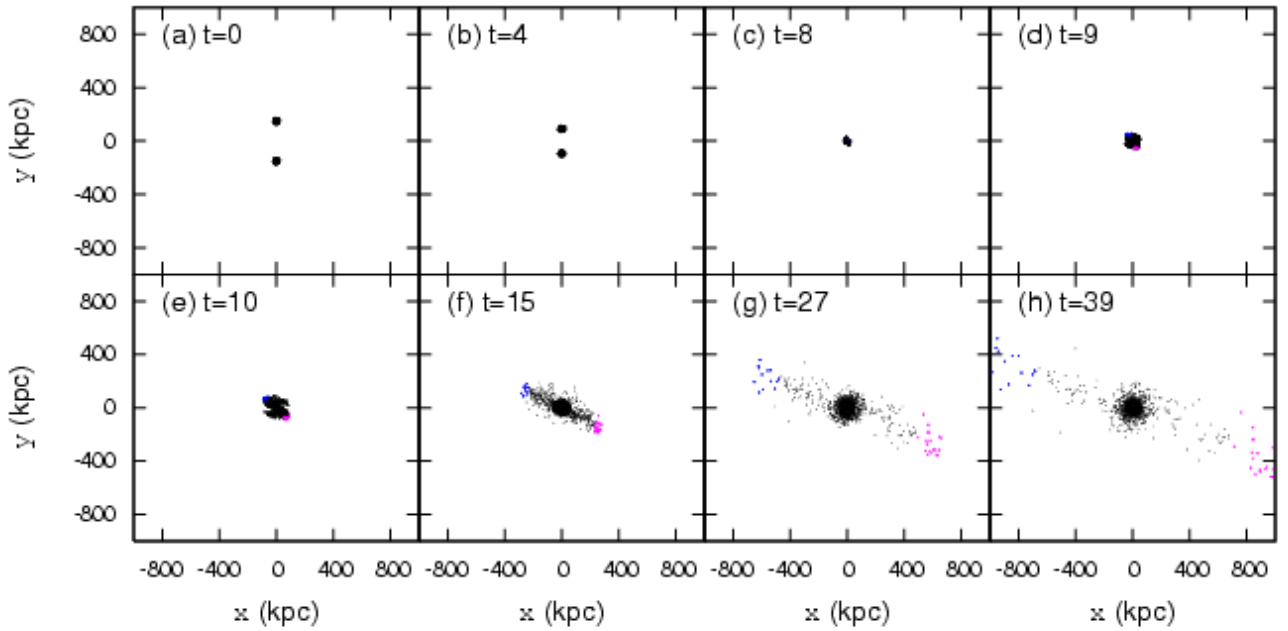


Fig. 4.— The distributions of stellar particles on the  $x - y$  plane in Model P1. (a)  $t=0$ ; (b)  $t=4 T_{dyn}$ ; (c)  $t=8 T_{dyn}$ ; (d)  $t=9 T_{dyn}$ ; (e)  $t=10 T_{dyn}$ ; (f)  $t=15 T_{dyn}$ ; (g)  $t=27 T_{dyn}$ ; (h)  $t=39 T_{dyn}$ . The blue dots represent the unbound particles which were belong to the galaxy initially located at  $(x, y, z) = (0, -150, 0)$ , and the pink dots represent the unbound particles which were belong to another galaxy.

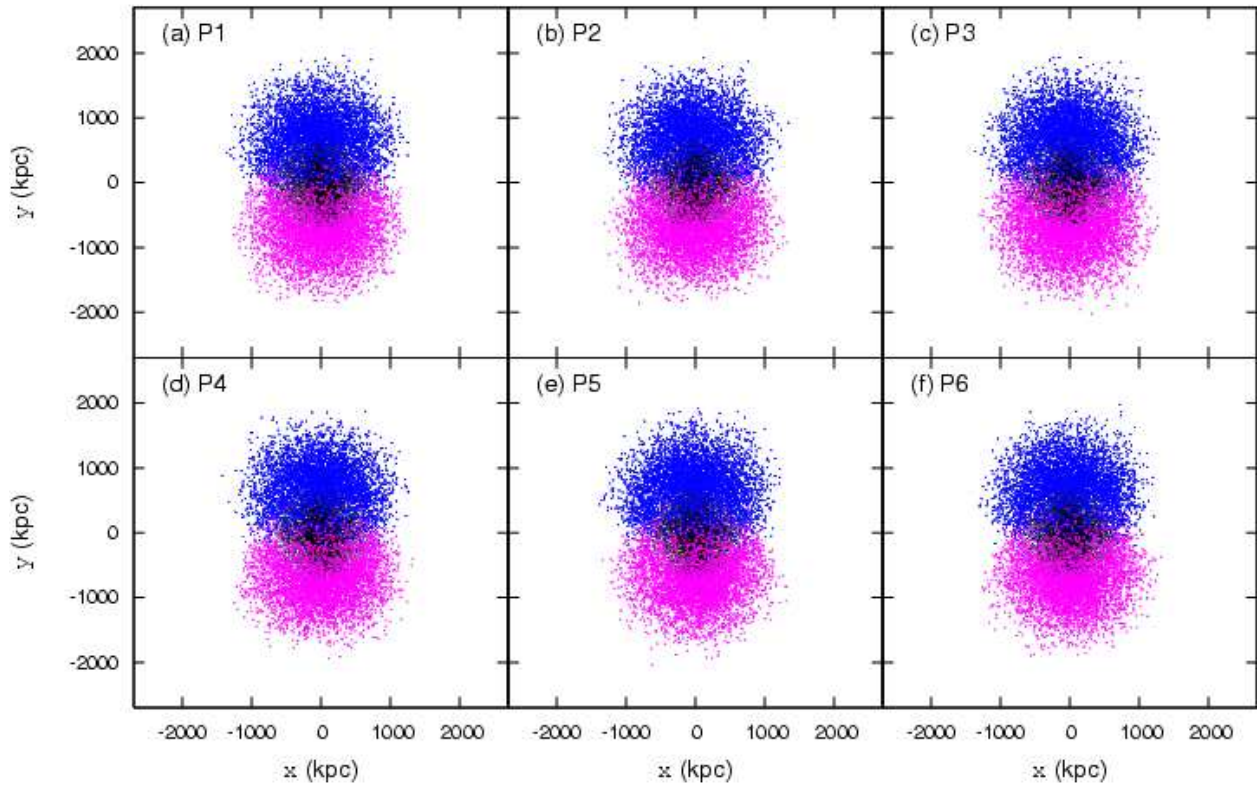


Fig. 5.— The distributions of halo particles on the  $x - y$  plane at  $t = 39T_{dyn}$  in Model P1-P6. The blue dots represent the unbound particles which were belong to the galaxy initially located at  $(x, y, z) = (0, -150, 0)$ , and the pink dots represent the unbound particles which were belong to another galaxy.

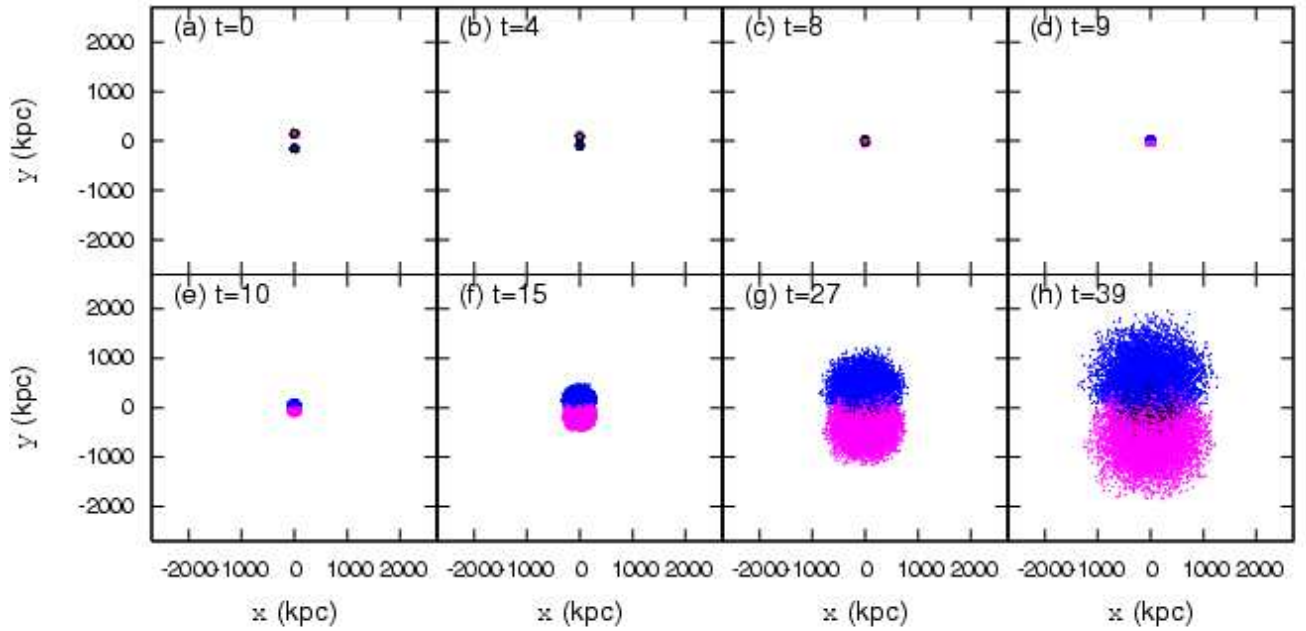


Fig. 6.— The distributions of halo particles on the  $x - y$  plane in Model P1. (a)  $t=0$ ; (b)  $t=4 T_{dyn}$ ; (c)  $t=8 T_{dyn}$ ; (d)  $t=9 T_{dyn}$ ; (e)  $t=10 T_{dyn}$ ; (f)  $t=15 T_{dyn}$ ; (g)  $t=27 T_{dyn}$ ; (h)  $t=39 T_{dyn}$ . The blue dots represent the unbound particles which were belong to the galaxy initially located at  $(x, y, z) = (0, -150, 0)$ , and the pink dots represent the unbound particles which were belong to another galaxy.

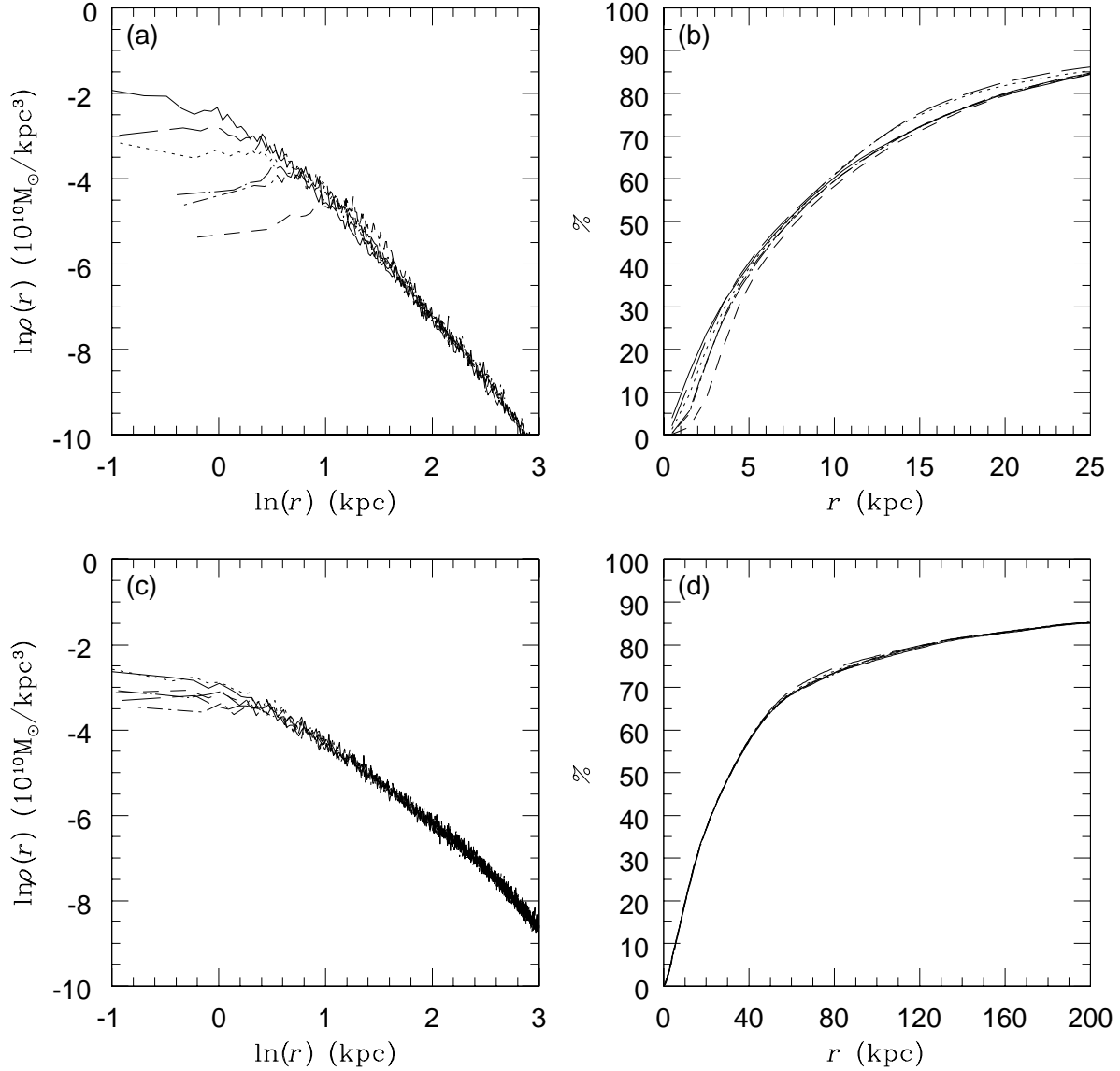


Fig. 7.— The profiles of parabolic mergers at  $t = 39T_{dyn}$ . (a) The density profiles of stellar components. (b) The percentage of stellar mass as a function of  $r$ . (c) The density profiles of dark-matter components. (d) The percentage of dark-matter mass as a function of  $r$ . The solid, dotted, short-dashed, long-dashed, dotted short-dashed, and dotted long-dashed curve is for Model P1-P6, respectively. The unit of  $r$  is kpc and the unit of  $\rho(r)$  is  $10^{10} M_{\odot} / \text{kpc}^3$ .

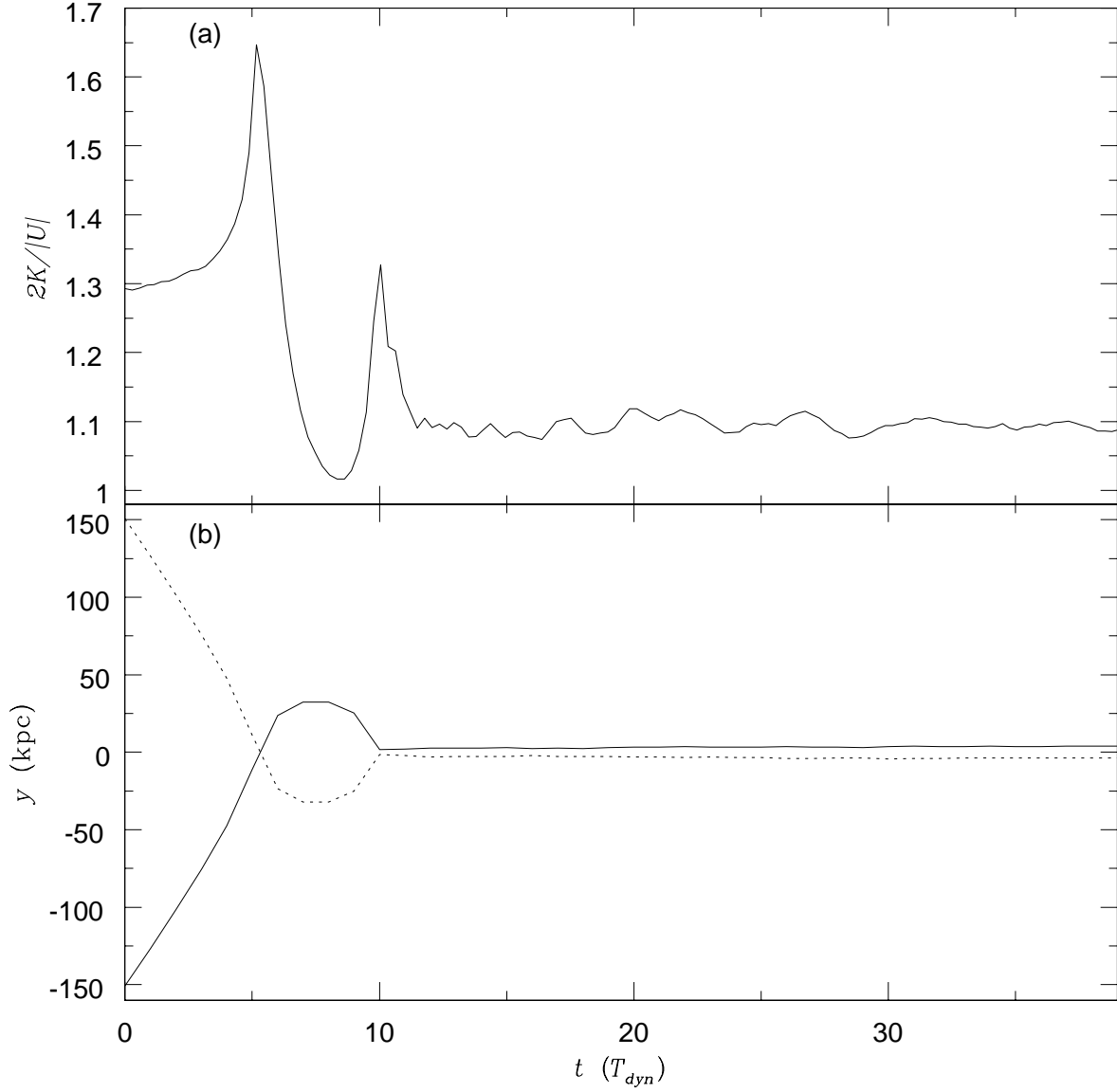


Fig. 8.— The evolution of Model H3. (a) The virial ratio  $2K/|U|$  of the merger as a function of time  $t$ . (b) The distance between two stellar components as a function of time during the merging process, where the solid and dotted curves are for the locations of two stellar components.

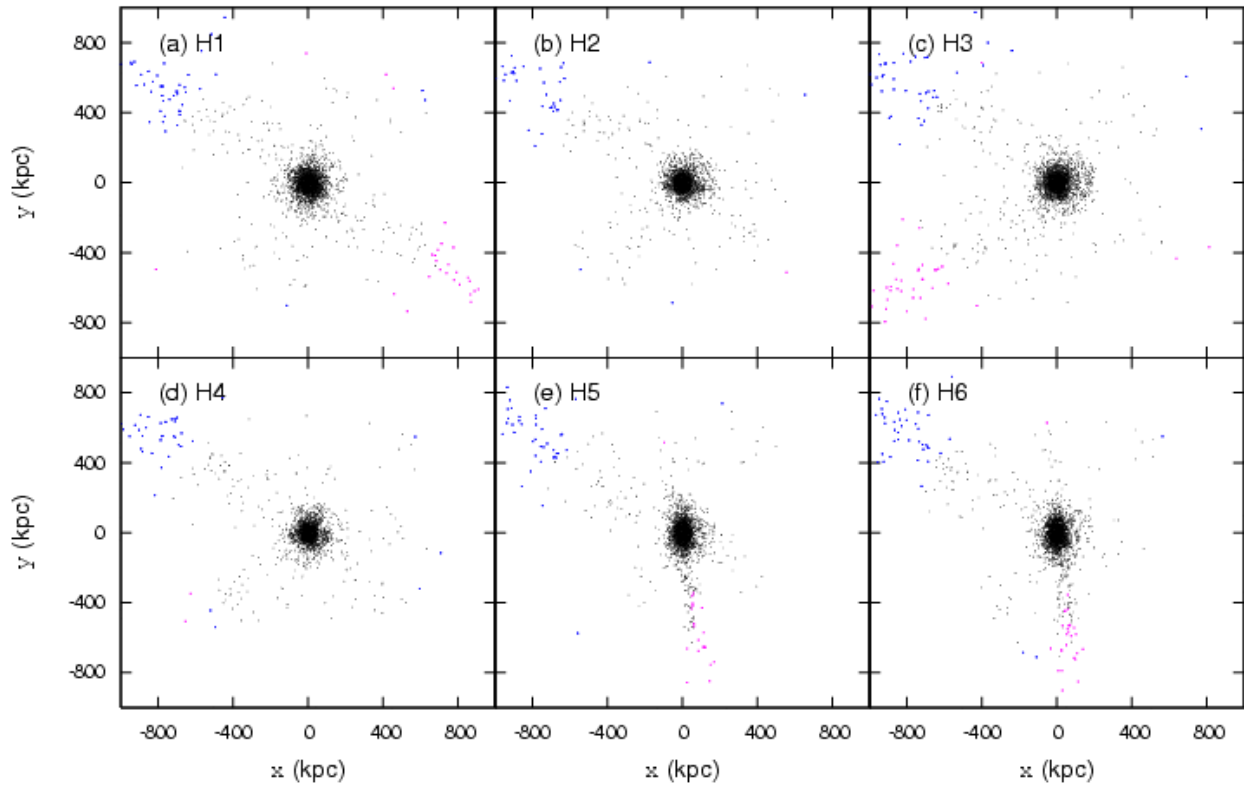


Fig. 9.— The distributions of stellar particles on the  $x - y$  plane at  $t = 39T_{dyn}$  in Model H1-H6. The blue dots represent the unbound particles which were belong to the galaxy initially located at  $(x, y, z) = (0, -150, 0)$ , and the pink dots represent the unbound particles which were belong to another galaxy.



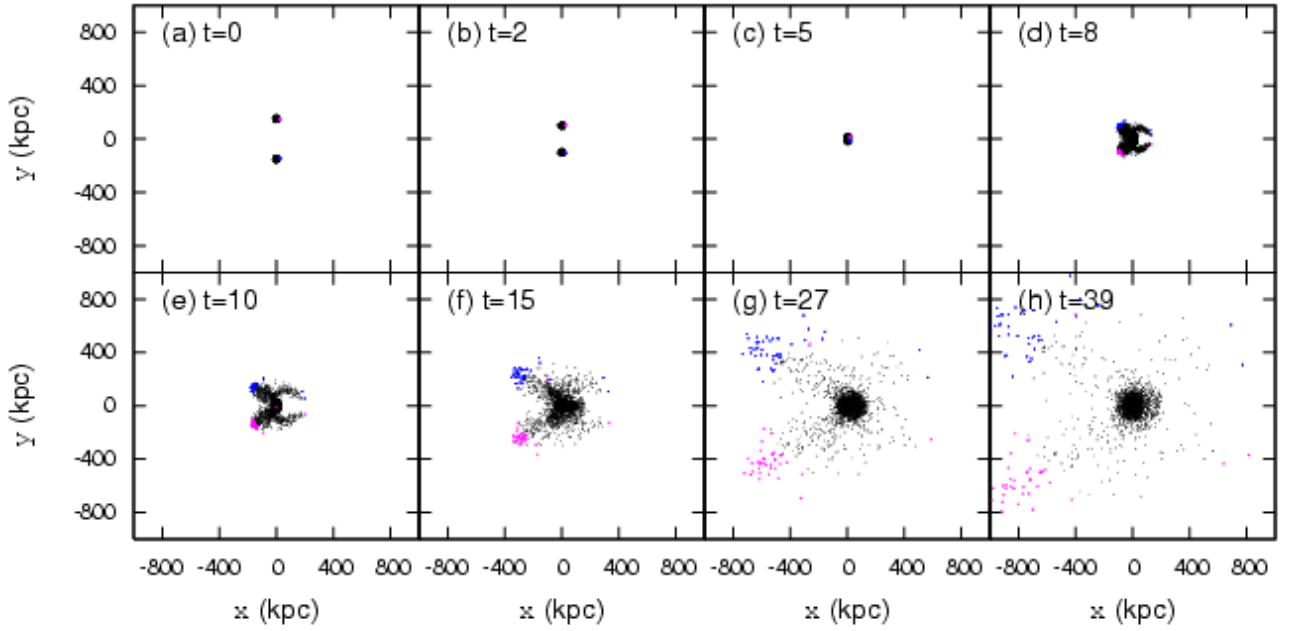


Fig. 10.— The distributions of stellar particles on the  $x - y$  plane in Model H3. (a)  $t=0$ ; (b)  $t=2 T_{dyn}$ ; (c)  $t=5 T_{dyn}$ ; (d)  $t=8 T_{dyn}$ ; (e)  $t=10 T_{dyn}$ ; (f)  $t=15 T_{dyn}$ ; (g)  $t=27 T_{dyn}$ ; (h)  $t=39 T_{dyn}$ . The blue dots represent the unbound particles which were belong to the galaxy initially located at  $(x, y, z) = (0, -150, 0)$ , and the pink dots represent the unbound particles which were belong to another galaxy.

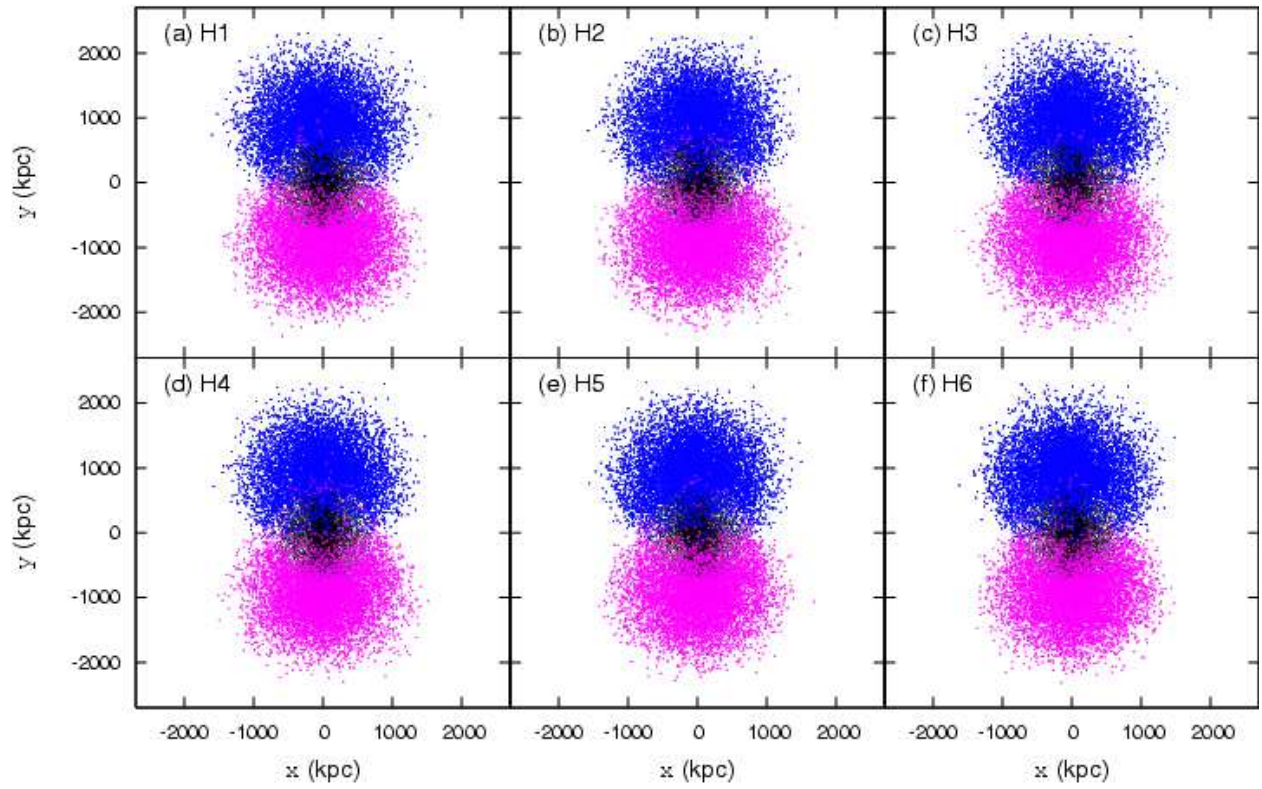


Fig. 11.— The distributions of halo particles on the  $x - y$  plane at  $t = 39T_{dyn}$  in Model H1-H6. The blue dots represent the unbound particles which were belong to the galaxy initially located at  $(x, y, z) = (0, -150, 0)$ , and the pink dots represent the unbound particles which were belong to another galaxy.

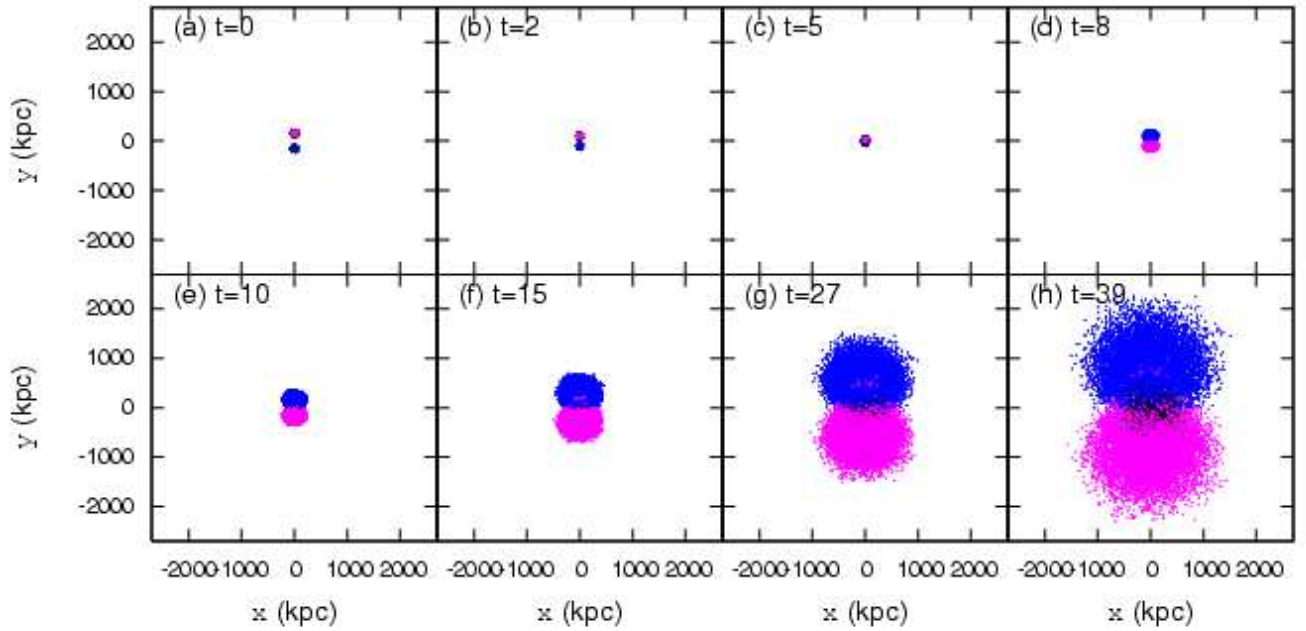


Fig. 12.— The distributions of halo particles on the  $x - y$  plane in Model H3. (a)  $t=0$ ; (b)  $t=2 T_{dyn}$ ; (c)  $t=5 T_{dyn}$ ; (d)  $t=8 T_{dyn}$ ; (e)  $t=10 T_{dyn}$ ; (f)  $t=15 T_{dyn}$ ; (g)  $t=27 T_{dyn}$ ; (h)  $t=39 T_{dyn}$ . The blue dots represent the unbound particles which were belong to the galaxy initially located at  $(x, y, z) = (0, -150, 0)$ , and the pink dots represent the unbound particles which were belong to another galaxy.

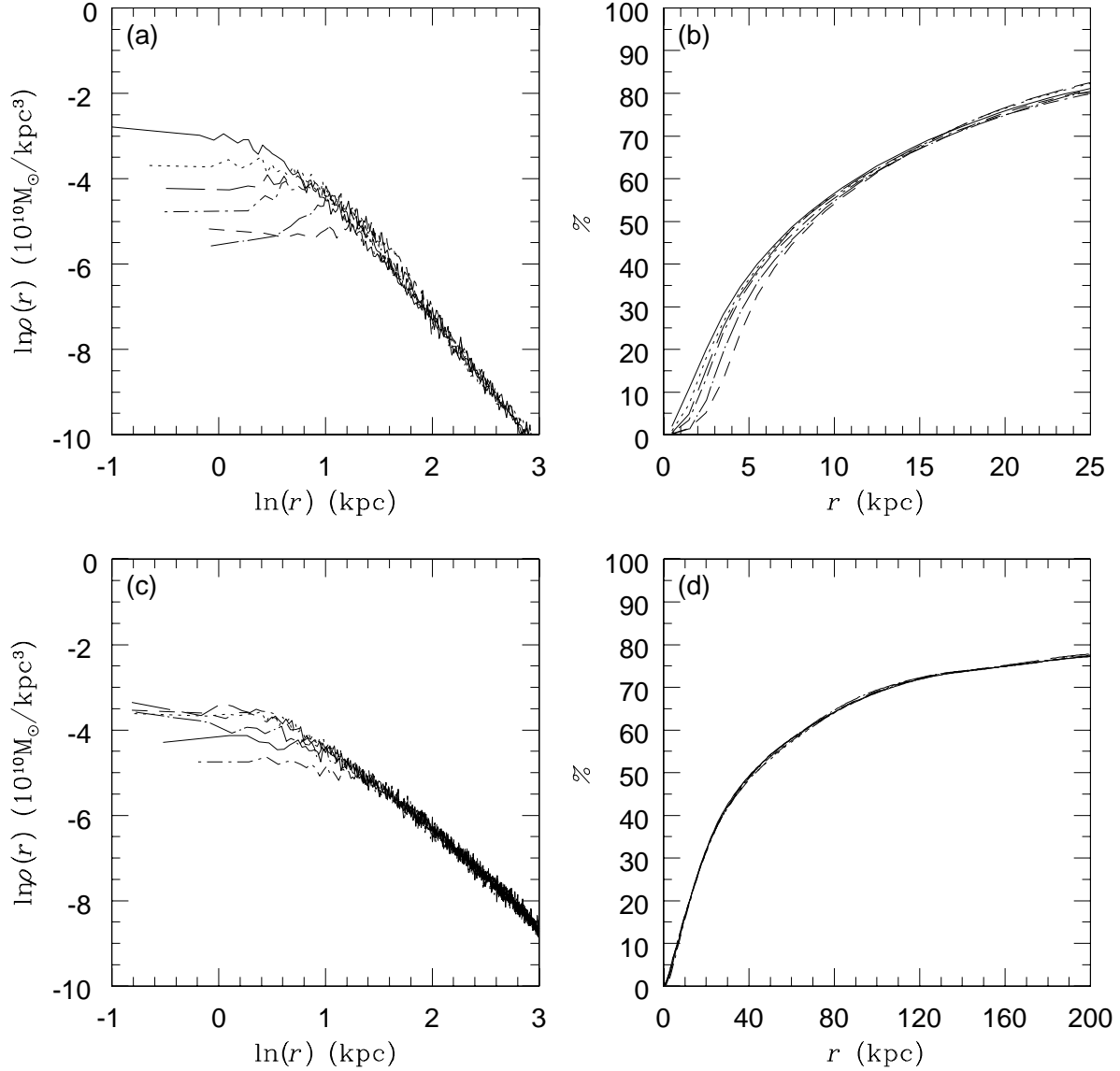


Fig. 13.— The profiles of hyperbolic mergers at  $t = 39T_{dyn}$ . (a) The density profiles of stellar components. (b) The percentage of stellar mass as a function of  $r$ . (c) The density profiles of dark-matter components. (d) The percentage of dark-matter mass as a function of  $r$ . The solid, dotted, short-dashed, long-dashed, dotted short-dashed, and dotted long-dashed curve is for Model H1-H6, respectively. The unit of  $r$  is kpc and the unit of  $\rho(r)$  is  $10^{10} M_{\odot} / \text{kpc}^3$ .

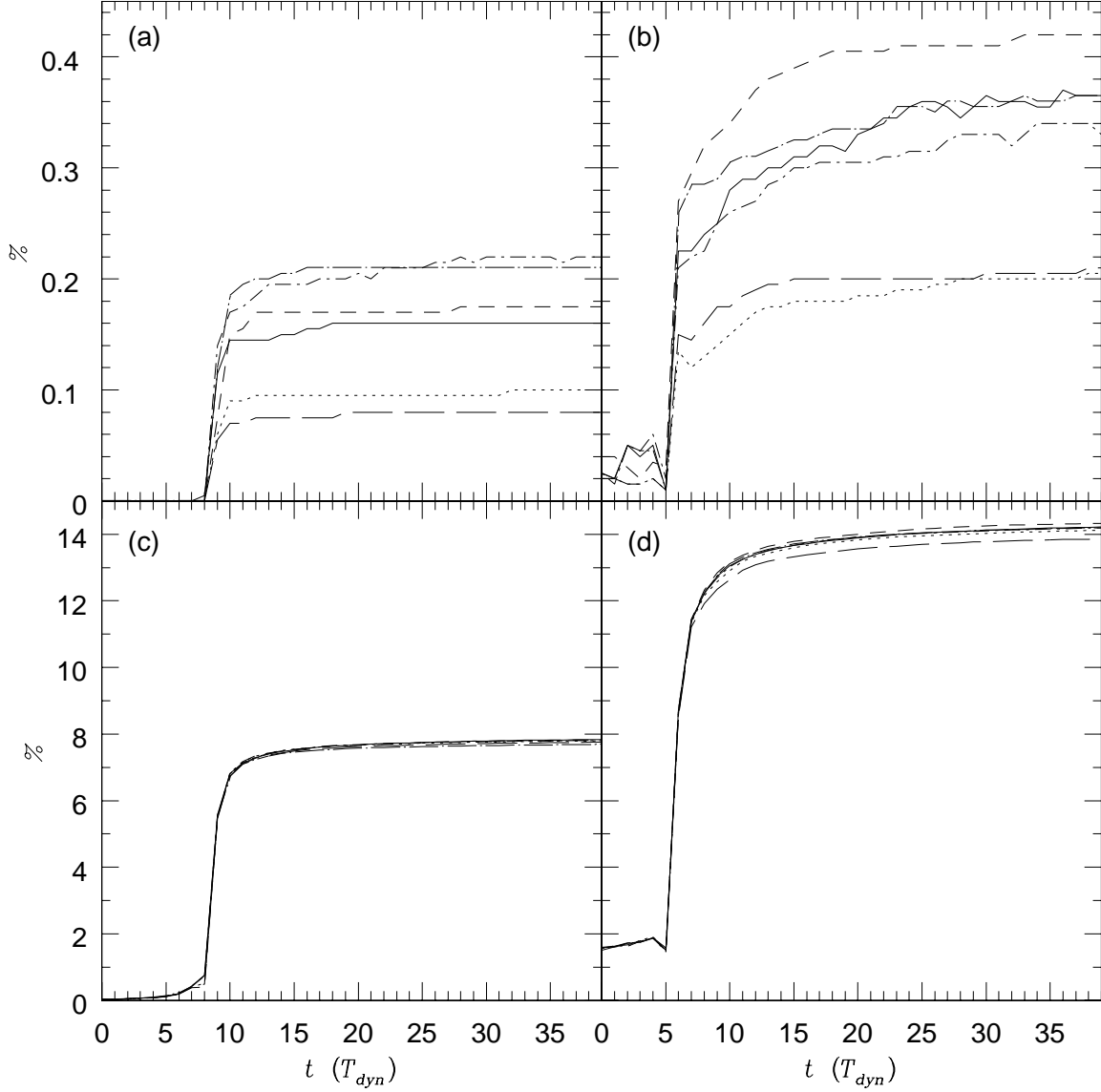


Fig. 14.— (a) The percentage of stellar GUP as a function of time in Model P1-P6. (b) The percentage of stellar GUP as a function of time in Model H1-H6. (c) The percentage of dark GUP as a function of time in Model P1-P6. (d) The percentage of dark GUP as a function of time in Model H1-H6. The solid, dotted, short-dashed, long-dashed, dotted short-dashed, and dotted long-dashed curve is for Model P1-P6 (H1-H6), respectively.